10th International Symposium on the Science and Processing of Cast Iron – SPCI10

Feeding Against Gravity with Spot Feeders in High Silicon Ductile Iron

N.K. Vedel-Smith[1*] and N.S. Tiedje[1]

[1]Department of Mechanical Engineering, Technical University of Denmark, Kgs. Lyngby, Denmark

A test pattern, with three different moduli castings was developed to investigate methods to optimise feeding of high silicon ductile cast irons. Different feeder types, modulus, and locations were investigated using both an insulating and an exothermal sleeve material. Porosities were analysed and classified using X-ray imaging and ultrasound analysis. The effect of the different feeder configurations were classified in reference to defect location, sleeve material, and feeder type, modulus, and location.

The analysis showed that exothermal feeder sleeves with the right configurations can feed up-hill against gravity. This effect may contribute to the thermal expansion created by the exothermal reaction. It was also found that the optimum feeder size does not scale linearly with the casting modulus but that larger casting modulus requires relatively smaller modulus feeders. The thermal gradient created by the feeders made with the insulating sleeve material was not sufficient to significantly improve feeding.

Keywords: ductile iron, spot feeding, risering, solidification, high silicon, ram-up sleeves.

Introduction

Feeding complex castings with different moduli sections is a challenge for the foundries, as customers require improved yield, less machining, and sound castings. Optimisation of cast components is an essential driver for many industries in order to improve their products. Thus the foundries are met with an ever growing requirement to improve methods and increase yield. The location and orientation of the casting is determined by casting geometry, location of cores and feeders. However, new designs with great variation between thin and thick walled sections, and highly complex designs limit the use of traditional feeders.

In vertically parted moulds geometrical feeders are normally located at the top of the casting on the parting plane. All feeders require an unbroken feeding path from the feeder to the section that must be fed. This makes it difficult, if not impossible, to feed heavy sections that are disconnected from the feeding path by a low modulus section. Additionally, the feeder requires a driving force to move the melt from the feeder into the casting. Traditionally this driving force is gravity, but other forces also act on the melt during solidification. E.g. solutions like the William wedge and similar geometries are a part of almost all feeder designs to ensure that the feeder is kept open to the atmosphere (punctured) and thus prevent the negative pressure gradient retaining the melt inside the feeder. Other natural forces working on the melt can be the contraction and expansion of the melt itself as different sections of the casting goes through the different stages of solidification at different intervals depending on the modulus, cooling rate, and alloy composition. The movement, deformation, expansion, and the reduction in strength of the green sand mould also influence these factors.

Descriptions and guidelines to the application and effect of feeders that make use of these naturally occurring driving forces to move the melt from a feeder located at the bottom of the casting into a section at a higher elevation are sparse at best. The study presented in this paper represents an experimental design comprising 9 different feeder configuration tested on a scalable casting geometry in three different sizes of casting moduli—8 mm, 10 mm and 15 mm. The study quantified the effect of different modulus spot feeders for different modulus castings. The trial was made with different insulating and exothermic ram-up sleeves together with high silicon ductile iron castings.

Experimental Procedure

Casting Geometry and Pre-feeder Design

The casting geometry was designed to be parametric in order to represent different moduli sections with the same geometry (see Figure 1). The casting itself was a rectangular cuboid. A square footprint was chosen because the square design allow for a high geometrical modulus and was better suited than a round design for ultrasound and x-ray analysis. The height of the casting was chosen as 3 times the width and depth of the casting. The basic idea with the design was to have one uniform section that would create a significant amount of shrinkage by itself. The height of the casting should be great enough that a feeder at the top and a feeder at the bottom would influence the casting differently due to the difference in ferrostatic pressure. For steel bars cast in a horizontal orientation the maximum feeding distance between two feeders was reported as varying between 1-4 times the thickness of the bar[1]. Though the trial castings are

* Corresponding author, email: nikvs@mek.dtu.dk

cast vertically and in SGI, it was chosen to uphold as great a distance between the two feeders on the casting as possible. The height of the bar was governed by the pattern size and allowed for a bar length of 3 times the thickness (a). In turn this allowed for a feeder distance of approximately 2.5 times the thickness (a).

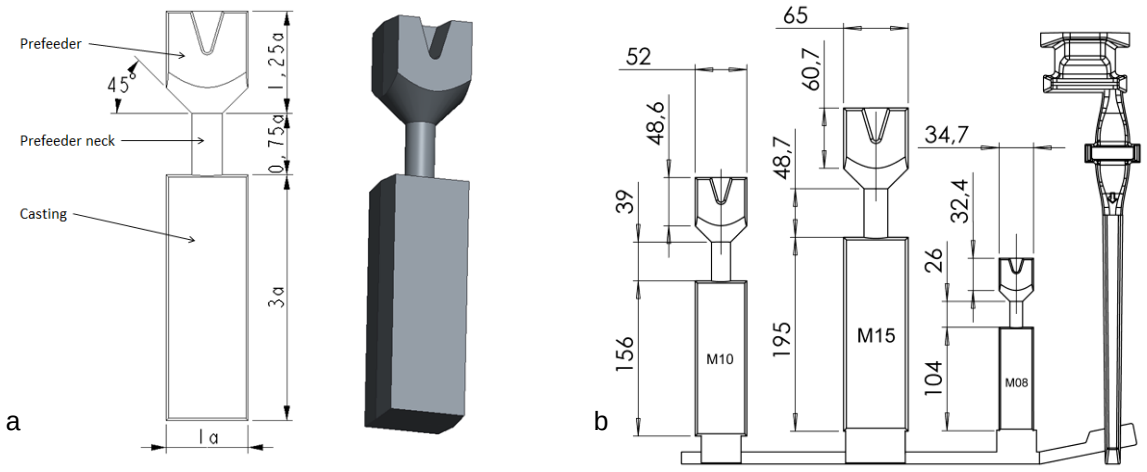

Fig.1: Schematic of the parametric casting design (a), and pattern layout (b). Measurements in mm.

A pre-feeder was placed on top of the casting—designed to compensate for the liquid shrinkage that occur as the casting cools from the pouring temperature to the solidus temperature, so that the variations in pouring temperature on total shrinkage are eliminated. The design had to ensure an identical amount of shrinkage in all castings, regardless of pouring temperature. If not done properly it would afterwards be impossible to prove that changes in porosities in the castings were related to changes in feeder configurations and not attributable to a smaller or greater liquid shrinkage caused by varying pouring temperatures.

The size of the pre-feeder neck was determined so that it closes and blocks feeding at the point in time where solidification begins in the casting itself. Based on Chvorinov's modulus law[2] equation (1) was derived:

$$D_{neck} = 4M_{neck} = \frac{c_p(T_{start}-T_{eut})}{(-\Delta H)+c_p(T_{start}-T_{eut})} M_{casting} \quad (1)$$

where D_{neck} was the diameter of the pre-feeder neck, M_{neck} was the modulus of the pre-feeder neck, and $M_{casting}$ was the modulus of the casting. H was the enthalpy of the system, c_p was the heat capacity, T_{start} was the pouring temperature and T_{eut} was the eutectic temperature for the given alloy. Equation (1) gives the diameter of the pre-feeder neck. However, the equation does not take into account the heat flux from the casting and pre-feeder but assume unidirectional solidification. To determine the optimum pre-feeder neck height, which would reduce the amount of liquid shrinkage as much as possible while still allowing for a timely solidification of the neck, numerical simulations of the different pre-feeder neck geometries were used (see Figure 2).

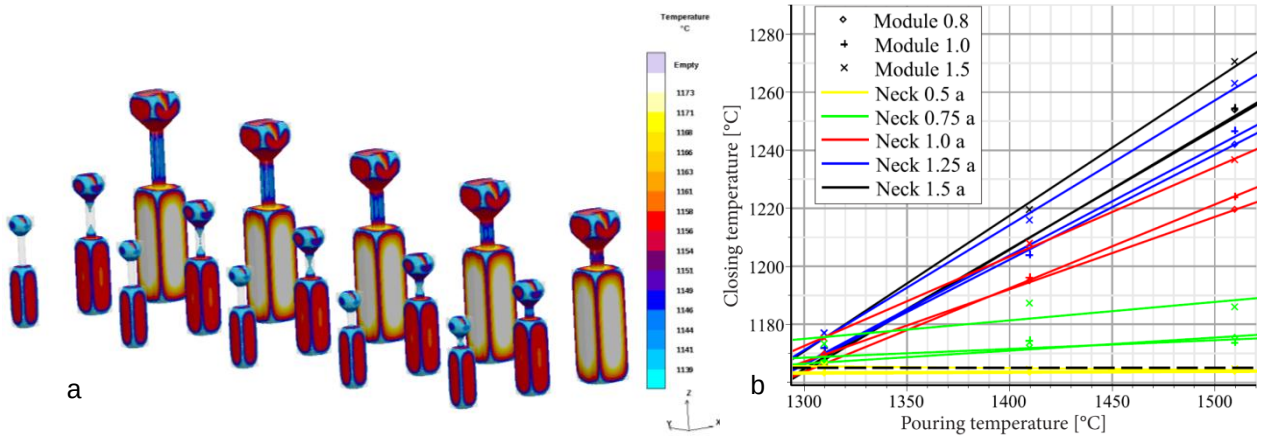

Fig.2: (a) Parametric study of varying pre-feeder neck lengths from 0.5a to 1.5a, and (b) a graph showing the temperature at the centre of the casting (Closing temperature) as a function of the pouring temperature for three different moduli castings and five different pre-feeder neck lengths. The dashed line indicates the eutectic temperature of the alloy.

The solidification times obtained from the numerical simulation of the different parametrical geometries, at different pouring temperatures, were plotted in Figure 2(b). The graph shows that the yellow line representing the shortest pre-feeder neck was below the eutectic temperature line. This means that the solidification of the casting had begun before the neck had closed off. All other pre-feeder neck lengths closed off before the casting centre reaches the eutectic temperature. Hence the pre-feeder neck length of 0.75a was chosen because that length allowed for the best prevention of liquid shrinkage and for the most uniform performance across all casting temperatures. Additionally, this analysis was repeated for another alloy with a different eutectic temperature to make sure the design would function with different alloy compositions.

Feeder Placement, Modulus, and Combinations

The trial setup consisted of 6 different feeder geometries, using either an insulating or an exothermic sleeve material, and applying feeders to two different locations on the casting—at the top near the pre-feeder neck (upper) and at the bottom near the ingate (lower). The possibility of placing feeders either at the top or bottom of the casting, or at both locations simultaneously, enabled an analysis of the feeders' performance in relation to the pressure height of the location. The feeders themselves were mounted horizontally, which minimises the feeders own influence on the ferrostatic pressure. The driving force for moving the melt from the spot feeder into the casting required other forces than gravity to act on the liquid in order to feed the casting. The horizontal orientation also minimised the difference between the upper and lower spot feeder location.

The different spot feeders were mounted onto the three different modulus castings as shown in Table 1. The first group (0) was a control group without any spot feeders. Groups 1 and 2 had only feeders at the upper location, groups 3 and 4 only at the lower location. The remaining groups (5-9) all had feeders at both the upper and the lower location. All combinations were cast in 2-3 duplicates to ensure repeatability.

Table 1: Trial combination overview. Numbers before the letter indicate melt volume [cm^3], letters indicate I for insulating and E for exothermic, and numbers after the letters indicate feeder modulus [mm].

	#	0	1	2	3	4	5	6	7	8	9	Feeder Types	
	Dup.	3	3	3	2	3	2	2	2	2	2	Ins	Exo
M08	U		28I08	28E10			28I08	07I05	28E10	08E08	07E06	07I05	07E06
	L				08E08	28E10	28E10	08E08	28E10	07E06	28E10	08I06	08E08
M10	U		22I10	22E12			22I10	08I06	22E12	28E10	08E08	28I08	28E10
	L				28E10	22E12	22E12	28E10	22E12	08E08	22E12	22I10	22E12
M15	U		121I16	121E19			121I16	22I10	121E19	82E15	22E12		82E15
	L				82E15	121E19	121E19	82E15	121E19	22E12	121E19	121I16	121E19

The spot feeders used in the study were so called ram-up sleeves which are mounted on a pin on the pattern before the moulding process begins. After the moulding process the ram-up sleeves are located inside the green sand mould as described by Vedel-Smith et.al.[3] Figure 3 show the spot feeders from group 6 mounted on the pattern, ready for moulding.

Fig.3: Spot feeders from group 6 mounted on the pattern, ready for moulding. Insulating spot feeders on the top. Exothermic spot feeders at the bottom.

Production, Alloy and Thermal Measurements

The castings were produced on a vertically parted moulding machine—Disamatic 240B—as part of a production run in an operating foundry. The mould size was 775 x 600 x 300 mm. The poured weight of the casting without any spot feeders was approx. 16 kg—whereof the M08 weights ~1.1 kg, M10 ~3.7 kg, and M15 ~7.3 kg. The pouring time was around 6 s. The castings were made with an EN-GJS-500-14[4] alloy and four alloy composition analyses were made during the duration of the trails. See Table 2.

Table 2: Alloy composition [wt%] and casting temperature [°C] variation during the trials.

	CE	C	Si	Mn	P	S	Mg	Cr	Ni	Mo	Cu	Sn	Temp [°C]
I	4.60	3.31	3.91	0.31	0.015	0.003	0.051	0.047	0.021	0.001	0.09	0.004	1,398 (±5)
II	4.57	3.31	3.81	0.31	0.015	0.003	0.045	0.046	0.023	0.001	0.09	0.005	1,387 (±5)
III	4.54	3.35	3.61	0.25	0.015	0.004	0.042	0.051	0.026	0.001	0.06	0.005	1,380 (±5)
IV	4.54	3.34	3.64	0.25	0.015	0.004	0.039	0.050	0.025	0.001	0.06	0.005	1,361 (±5)
Avg	4.56	3.33	3.74	0.28	0.015	0.004	0.044	0.049	0.024	0.001	0.08	0.005	1,382 (±5)

Four temperature measurements were made in one of the castings—4A—which was cast immediately before the series II castings listed in Table 2 were made. Three thermo couples were placed at the centre of each parametric casting, and a single thermo couple was placed at the lower spot feeder of the M15 parametric casting (see Figure 4). All thermo couples were K-type and the data were recorded at a sampling rate of 1 Hz with a stand-alone 4-channel thermo couple data logger.

The castings solidified and cooled in the mould for approx. 1½ hours, and were thereafter removed manually from the moulds at the shake-out station. This ensured that all spot feeders remained attached to the castings. When the castings had air cooled to room temperature they were cleaned by shot blasting.

Ultrasound Analysis and X-ray Analysis

All castings were analysed with ultrasound by the same, experienced operator using a Karl Deutsch Digital-Echograph. The location and size of the porosities were painted on the castings. This gave a detailed picture of the size, location, and direction of the porosities. All castings were photo documented for later analysis.

Following the ultrasound analysis selected groups of castings were analysed using x-ray imaging. The x-ray imaging focussed on confirming the results obtained by the ultrasound analysis, but also on documenting the porosities located in areas not suitable for ultrasound analysis—the pre-feeder neck and the spot feeders. Several images were taken of each of the castings and then assembled into an overview, allowing for a more holistic analysis of the x-ray imaging results.

Results

Ultrasound Analysis

The findings from the ultrasound analysis were classified with respect to porosity size (0-4 where 0 is no porosities and 4 is large porosities), porosity location (top, middle, bottom), and if porosities at different locations were connected or disconnected. Additionally it was also registered when the porosities had an opening out unto the surface of the casting (**bold**). See Table 3.

Table 3: Results of the ultrasound analysis

	#	0			1			2			3		4			5		6		7		8		9	
		A	B	C	A	B	C	A	B	C	A	B	A	B	C	A	B	A	B	A	B	A	B	A	B
M8	T	4	4	4	4	4	4	4	4	4	4	4	4	4	4	4	4	4	4	0	2	4	4	4	3
	M	2	2	2	2	2	0	0	0	0	2	2	2	2	2	2	2	0	0	2	2	4	4	4	4
	B	0	0	0	0	0	0	0	0	4	0	0	0	0	0	0	0	0	0	2	0	0	0	0	0
M10	T	4	4	4	4	4	4	4	4	4	4	4	4	4	4	4	4	4	4	4	4	4	4	4	4
	M	2	2	2	1	0	1	2	2	0	2	2	2	2	2	2	2	2	2	2	2	2	2	2	2
	B	0	0	0	0	0	0	0	0	0	0	0	0	0	0	0	0	0	0	0	0	0	0	0	0
M15	T	4	4	4	4	4	4	4	4	4	0	0	0	4	4	4	4	0	0	2	2	1	0	0	0
	M	0	4	2	0	2	1	0	0	0	1	3	2	4	4	0	2	2	1	0	0	0	0	1	0
	B	0	0	0	0	0	0	0	0	0	0	0	2	4	4	0	0	0	0	0	0	0	0	0	0

	Nomenclature
0	No porosity
1	Micro Porosities
2	Small Porosities
3	Medium Porosit.
4	Large Porosities
	Connected
	Disconnected
	Puncture at neck

The quantified results of the ultrasound analysis indicated that many of the different castings, especially the two smallest modulus castings, displayed the same amount of porosity as the reference casting groups (0) without any spot feeders. This was partly true, however it should be noted that the large porosity (4) indication has no upper limit, meaning that the same indication can cover great differences (see Figure 4).

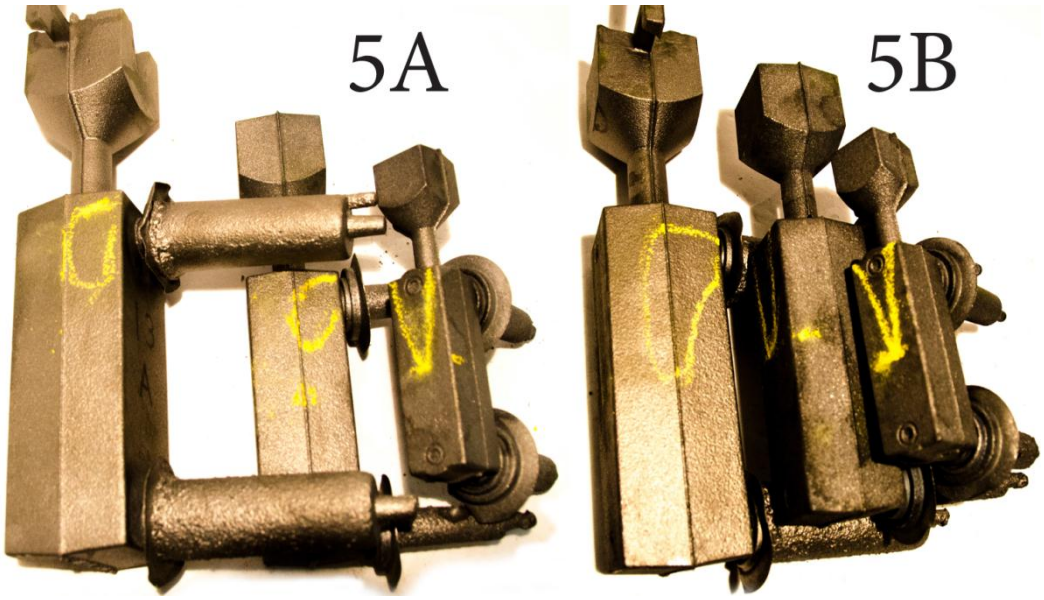

Fig.4: Porosity markings from the ultrasound analysis of casting groups 5A and 5B.

Additionally, some of the reference castings without spot feeder displayed clear signs of surface shrinkage, indicating that some of the shrinkage for these castings have occurred in location that have not been covered by this analysis. Surface shrinkage was not observed in any of the castings with spot feeders.

X-Ray Imaging and Analysis

The x-ray images are greyscale images produced by irradiating the casting from one side, and recording the radiation that reaches the sensor at the opposite side. This gives an image that in greyscale contrast show areas with little material in between (light), and areas with a lot of material in between (dark). Porosities show up because they are holes in the bulk material, and thus areas with porosities absorb less radiation, resulting in a brighter area of the image. However, the radiation does scatter and diffuse, rendering the images a little fuzzy at the edges. Because of this effect there was a limit to the difference between the size of the casting and the size of the porosity that could be imaged. This made it difficult to obtain good images of the defects in the M15 castings (see Figure 5).

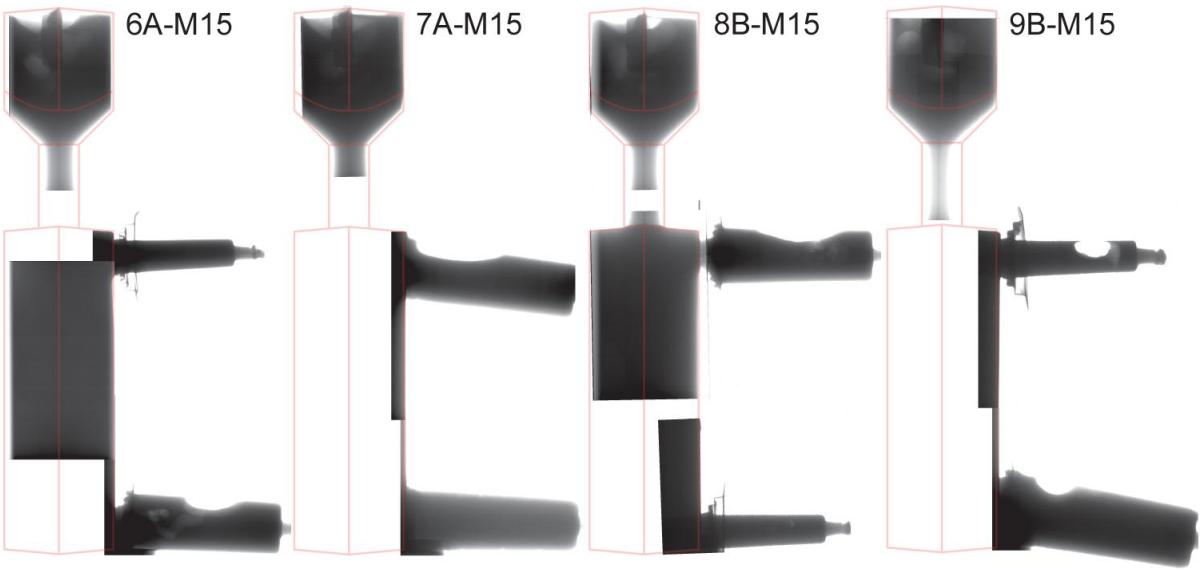

Fig.5: X-ray images of casting 6A, 7A, 8B, and 9B—all that largest casting with a modulus of 15 mm.

Thermal Measurements and Cooling Curves

The cooling curves showed that the three parametric castings solidified and cooled in a comparable manner, confirming that the parametric design provide the intended comparison between the different moduli castings (see Figure 6). The maximum temperature measured was 1,325 ±5 °C indicating that the gating filling of the mould has lowered the temperature of the melt by 62 ±10 °C from the pouring temperature of 1,387 ±5 °C. However, the specified temperature limit of 1.300 °C for the K-type thermo couples for short duration readings should be taken into consideration[5].

The cooling curves showed that in the bottom part of the M15 casting ended solidification approx. 320 s before the centre of the casting, albeit 400 s later the curves met again. This was caused by the thermal influence of the spot feeder, and the area between the two curves indicates the energy that the spot feeder provides transferred to the casting.

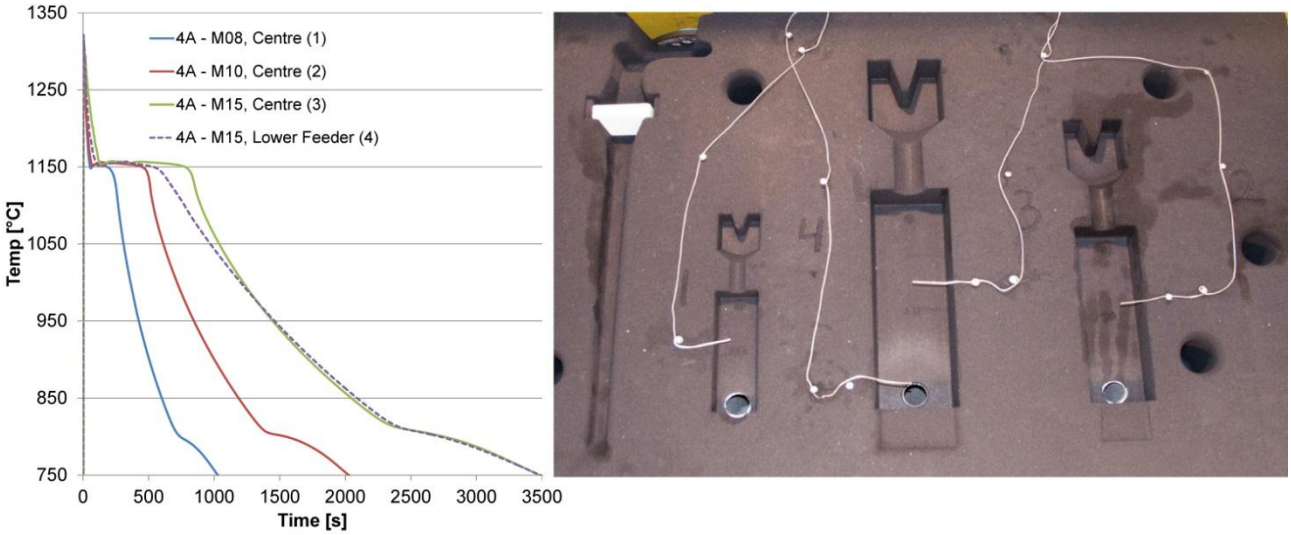

Fig.6: Thermal measurement of the casting, cooling, and solidification of casting group 4A.

Discussion

Examining Table 3 it was seen that most of the castings, regardless of modulus size and spot feeder combinations, had a large (size 4) porosity at the top and a small (size 2) porosity at the middle. As mentioned in the results section the large porosity characteristic was open ended, and covered many gradually increasing porosities. However, the consistent results show the stability of the model and the production conditions. Thus, the most interesting castings were the ones that differentiate from the stable and repeatable porosities formed in the other castings.

Castings 8B-M15 and 9B-M15 were classified as porosity free and the castings with the same spot feeder configuration—8A-M15 and 9A-M15—only displayed micro (size 1) porosities. 7A-M15 and 7B-M15 were classified with small porosities at the top, but no porosities at the middle. Finally, 3A-M15 and 3B-M15 only displayed porosities at the middle of the casting—ranging from micro (size 1) to medium (size 3) porosities.

The smaller castings—M08 and M15—did not show the same effect for these feeder configurations even though the modulus of the spot feeders were scaled according to the changes in casting modulus. This indicated that the solidification of the three different modulus castings was different as well. These changes in solidification can be caused by the slower solidification of the large modulus castings, which provide the longer time for the graphite nodules to grow and inhibit pearlite formation which would have reduced the effect of the graphite expansion. However, the high Si content of the alloy greatly limits pearlite formation already, and none of the three castings are small enough to be considered thin walled sections. Hence other factors were needed to fully explain the solidification differences between the different modulus castings.

Additionally several of the castings had ‘punctures’ at the bottom of the pre-feeder neck, opening into a large porosity in the casting. This effect seemed to have been dominant for the smaller modulus castings, but it also seemed to be unrelated to the amount of porosities recorded and the effectiveness of the spot feeders.

The most likely explanation was that the large modulus castings had a greater tendency to form a solid shell early during solidification, so that the low pressure that occurred inside the casting towards the end of solidification had enough force to move the melt from the spot feeders and into the casting itself.

Some melt may have been provided by the pre-feeder regardless of the intention that this should not happen. The x-ray images showed that the pre-feeders contained porosities. It was not possible to determine how much of the porosities in the pre-feeders that was a result of feeding and how much were related to the liquid shrinkage that the pre-feeders were designed to handle. However, it was noted that most pre-feeders displayed the some amount of porosities.

No correlation was found between the amount of porosities in the pre-feeder and the amount of porosities in the casting itself.

However, the negative pressure gradient from the casting itself could completely explain the results shown in Table 3. If group 3 and 4 were compared for the M15 castings it was noted that the first displayed a few and small porosities whereas the latter displayed more and larger porosities. However, it was the latter—group 4—that had the largest spot feeder. If the main driving force for feeding from the spot feeder into the casting was the negative pressure in the casting, then the larger spot feeder should have produced a porosity free casting. Instead it was seen that the smaller spot feeder reduced the porosities in the casting significantly compared to the large one.

To explain this phenomenon other forces than a negative pressure caused by shrinkage of the material in the casting must be taken into account. The graphite expansion was assumed to be the same for both configurations as they were cast with the same alloy, and only minor differences would occur as an effect of the small changes in solidification between the two spot feeder configurations. However, the timing of the graphite expansion, and particularly in relation to the timing of the negative pressure inside the casting, seemed to reach an optimum for this configuration. Thus, the two different forces come to act together, rather than against each other. If so, this could be seen as a special case of John Campbell's feeding rule no. 6 regarding the pressure gradient requirement[6].

External forces can also have occurred and gas development from exothermic feeder sleeves was a known concern. However, if gas development from the exothermic material was a significant driving force for the movement of the melt, then group 4 and 5 should have displayed fewer porosities than what was recorded.

Finally, examining the results of the M15 casting groups 3, 6, 8, and 9, in comparison with the other five groups, it was shown that a feeder located at the lower part of a casting section can feed the section with equal efficiency compared the same feeder located at the upper part of the casting section. This showed that the horizontally oriented spot feeders with exothermic sleeve material depend little upon the gravity as a driving force for feeding.

Conclusions

1. The optimum feeder size did not scale linearly with casting modulus. Larger casting modules required relatively smaller modulus feeders.
2. The timing of the negative pressure from solidification shrinkage combined with the timing of the graphite expansion seemed to be important in order to achieve the best possible feeding conditions. Similarly a larger feeder may shift the time enough for the effects to counteract each other and thus cancel most of the feeding effect if not directly developing more shrinkage.
3. The location for horizontally oriented spot feeders was relatively unaffected by the difference between the high and low location. The spot feeders that functioned at one location also functioned at the other location. The spot feeders that did not function at one location did not function at the other location either. In special cases it was possible to feed against gravity.

References

1. ASM International: Casting Design and Performance–Part II: Process Design, Riser Design, 2009, 61-72.
2. N. Chvorinov: Theory of the Solidification of Castings, *Giesserei*, Vol. 27, 1940, 177-186.
3. N.K. Vedel-Smith, N.S. Tiedje, K.T. Maza, and J. Sällström: Quantification of Feeding Effects of Spot Feeding Ductile Iron Castings made in Vertically Parted Molds, AFS Proceedings, 13-1310, 2013.
4. EN 1563:2012-3: Founding: Spheroidal Graphite Cast Irons, 2012.
5. L. Michalski, K. Eckersdorf, J. Kucharski, and J. McGhee: Temperature Measurements, 2nd Edn, 2001 John Wiley & Sons Ltd.
6. J. Campbell: 'Casting Practice – The 10 Rules of Castings', 120-156, 2004, Burlington, Elsevier Butterworth-Heinemann.

Acknowledgement

This work was funded by the Public Service Obligation (PSO) funds made available by the Danish Government. The project was made in collaboration with FOSECO Ltd., MAGMA GmbH, DISA Industries A/S, and Vald. Birn A/S. Rune Engelberth Hansen carried out the development of the parametric casting geometry.